

Numerical and Experimental Study of Crack Propagation in the Tensile Composite Plate with the Open Hole

Pawel Wysmulski¹

¹ Lublin University of Technology, ul. Nadbystrzycka 38D, 20-618 Lublin, Poland

E-mail: p.wysmulski@pollub.pl

ABSTRACT

In this study, the thin-walled plate with the central open hole made of carbon-epoxy composite was investigated. The plate was tested in tension to investigate the mechanism of crack formation in the composite structure. The studies were carried out using two individual methods: experimental and numerical. In the experiment test, load was measured as the function of plate elongation. The Plate elongation was analysed using the Aramis optical non-contact measurement system. In the numerical study, the FEM model reproducing the experimental conditions was developed in the Abaqus software. The cracking process was modelled using the XFEM method (extended finite element method). This procedure allowed the of the composite to be examined over the full range of the tensile load. The behaviour of the plate with a circular open hole was investigated before damage symptoms and the damage initiation load was determined. The study continued to analyse the initial cracking and delamination of the laminate layers, together with crack propagation leading to cracking of all the laminate layers (complete failure of the composite structure). The novelty of this study is that it uses the popular XFEM method to describe the cracking and failure of the composite structure. In addition, the study proposes the novel method for determining the crack initiation and failure loads of the composite plate under tension, and the results obtained thereby are verified numerically.

Keywords: crack propagation, laminates, thin-walled structures, finite element method, XFEM, tensile analysis.

INTRODUCTION

The use of modern material technologies and advanced manufacturing methods in a design of thin-walled structures makes it possible to obtain structures with enhanced operational and strength properties. Thin-walled structures are used many industries, including the automotive, aerospace and currently expanding yacht industry [1,2]. The significant improvement in the stiffness and strength properties of structural elements is achieved by replacing previously used standard construction materials with modern composite materials. This group of composites mainly includes polymeric laminates reinforced with continuous fibres, predominantly CFRPs (carbon fibre-reinforced polymers) and GFRPs (glass fibre-reinforced polymers). They are mainly used in thin-walled shell stiffeners, which are usually

designed as open and closed profiles with complex cross-sectional profiles. The scientifically proven beneficial mechanical properties of these materials combined with their low mass make it possible to use these materials in the manufacture of load-bearing elements for structures that are subjected to complex operational load conditions [3–5]. Laminates make it possible to shape the mechanical properties of designed components in terms of their ability to carry a specified type of load [6–8]. This feature makes it possible to achieve highly advantageous structural designs; this, however, requires a use of modern testing methods that allow an examination of the performance of the structure in the full load range [9–12]. Previous studies on composite structures predominantly concerned analytical and numerical analyses of structures with standard cross sections under simple loads. These considerations

have only been verified to a limited extent by experimental tests carried out on actual structural components [13–15].

In fibre laminates the stress state depends on the fibre configuration and varies from layer to layer, which makes it a complex problem. For this reason, the stress concentration induced by a hole in the laminate varies from layer to layer, and the general stress concentration factor specified for isotropic materials cannot be used in cases of this type (the classic Kirsch problem [16]). In the author's opinion, this condition can be described numerically since – as it is known from scientific publications – the occurrence of holes in thin-walled structures is unavoidable, if only for technological requirements [17–19]. The complexity of the above issue resulting from the possibility of shaping the properties of laminated composites makes this research problem still valid. In the literature one can find studies [20–22] which propose solutions to the problem of hole formation in composite materials.

The XFEM eliminates the need for a conformal FEM mesh [23]. The XFEM method (extended finite element method) was first described by Belytschko and Black [24]. This is an extension of the traditional finite element method using the concept of unity division developed by Melenka and Babuski [25]. This allows for easy integration of local enrichment functions with the FEA approximation. The existence of discontinuities is ensured by specially enhanced functions in combination with additional degrees of freedom. The finite element structure and its properties, such as sparsity and symmetry, were, however, retained. The use of XFEM must be complemented by adequate mesh densification near the crack tip. The XFEM method also ensures that crack initiation and propagation along the path could be examined without the need to re-discretise the numerical model [23, 26]. The enrichment functions consisting of asymptotic near-tip functions are used for crack analysis. The asymptotic singularity functions only taken into account in stationary crack modelling using Abaqus/Standard [27]. In contrast, the moving cracks are modelled using alternative approaches: the cohesive segment approach or the linear elastic fracture mechanics (LEFM) approach [28–30]. With these techniques, crack initiation is defined up to the onset of cohesive degradation of the enriched component, and the degradation stage is reached when the strains or stresses meet the defined crack initiation criteria.

This paper deals with a quantitative and qualitative determination of a fracture behaviour of a thin-walled CFRP plate with a central circular hole in tensile testing [31–33]. The study focuses on providing the detailed description of a cracking mechanics of the carbon-epoxy composite structure [34–36]. The failure process is described by independent test methods over the full load range, from damage initiation through crack propagation to the full failure of the composite structure [46–49]. The tensile plate with a hole was investigated both experimentally and numerically by the FEM. This focus has enabled the development of numerical models that reproduced real structures [41–44]. As part of the study, a method for determining the load initiating the fracture and failure of the tensile composite plate was developed and numerically verified. It is worth mentioning that the study uses the now very popular FEM method, which is widely used in many fields of science [45–49]. The novelty of the research problem undertaken in this study is that it describes the phenomenon of fracture and the failure of composite structures using a currently popular XFEM. A literature review demonstrates that numerous studies were devoted to the application of XFEM for isotropic materials [50–53]. However, there is a lack of studies describing the failure of real layered composites (CFRP) using the numerical XFEM technique. The FEM model developed based on experimental findings may be used to analyse the failure process of this type of composite structures.

TEST SPECIMEN AND ITS MECHANICAL PROPERTIES

The test object was the thin-walled laminate composite structure weakened by an oval hole. The hole was cut in the specimen to weaken the structure and cause the composite material to fracture in a specified region during the tensile test. The plate was made from the unidirectional HeXPly prepreg strip (from Hexcel) of carbon fibre-reinforced composite with epoxy matrix [54–56]. The polymerisation process was conducted in an autoclave, the curing process lasted 2 hours and was characterised by a package vacuum of 0.08 MPa, with the overpressure and autoclave temperature set to 0.4 MPa and 135 °C. The analysed laminate structure had a symmetrical fibre lay-up configuration of the composite layers [0/90/0/90₂/0/90/0].

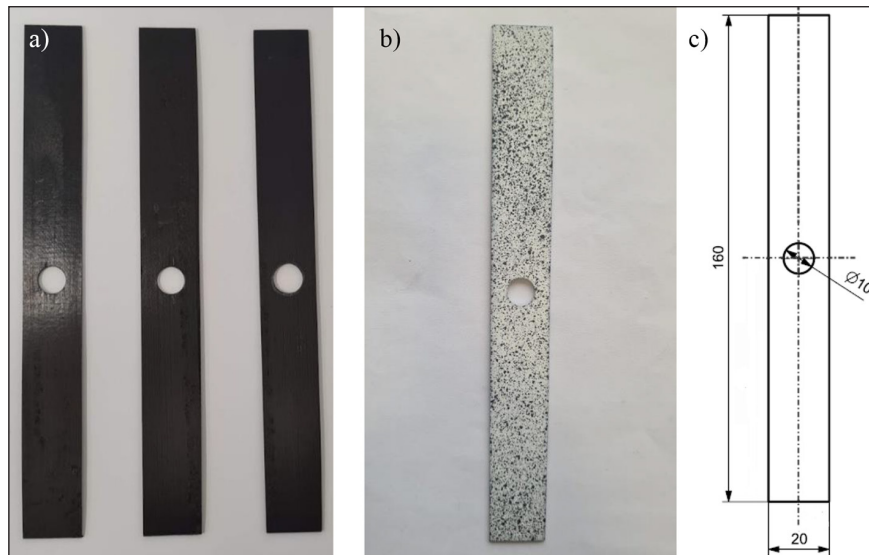


Fig. 1. Test object: a) real composite panels with a hole, b) specimen with contrast patterning, c) scheme showing the dimensions of a specimen and a hole

Table 1. Mechanical properties of carbon-epoxy composite

E_1	$E_{2,3}$	$G_{12,13,23}$	$\nu_{12,13,23}$	F_{T1}	F_{T2}	F_S	F_{C1}	F_{C2}
GPa	MPa	MPa	–	MPa	MPa	MPa	MPa	MPa
130.71	6360	4180	0.32	1867.2	25.97	100.15	1531	214

Figure 1a shows the samples prepared for experimental testing. The thickness of the test plate was 1.048 mm. The scheme in Figure 1c shows the dimensions of the specimen and of the central hole. In addition, contrast patterning was applied to the specimens to enable the use of a non-contact optical measurement method in the experiments, as shown in Figure 1b.

Table 1 shows the mechanical properties of the layer of the CFRP laminate in three orthotropic directions: G - shear modulus, ν - Poisson’s ratio, E - tensile modulus, F_T - tensile strength, F_S - shear strength, and F_C - compressive strength. The properties of the carbon-epoxy composite were determined experimentally in compliance with the relevant ISO standard [57]. This made it possible to determine a actual mechanical properties of a produced material, as in practice these may differ from the ideal properties declared by the manufacturer. The determined properties were then used to define the numerical model of material which was conducted using Abaqus and finite element method.

METHODOLOGY OF THE EXPERIMENT

The manufactured plates with a central oval hole were subjected to axial tensile testing. The

experimental tests were conducted using the Comotech QC-505 M2F typical testing machine having a load cell with a range of up to 50 kN and an accuracy class of 0.5% (Fig. 2a:3). Specially designed wedge grips with facings for flat specimens with a thickness ranging 0.2–11 mm were attached to the pins of the testing machine (Fig. 2a:2). These were used to clamp the test specimen which was inserted axially 20 mm into each of the upper and lower wedge grips. This made it possible to obtain a test area of 20×120 mm on the plate (Fig. 2a:1). In the tensile test, the load and elongation of the plate were measured at a constant crosshead speed of 1mm/min. In addition, the displacement of the composite structure in the frontal plane of the plate over time was recorded using the Aramis optical measuring system (Fig. 2a:4). This system is equipped with a 20M resolution camera (5472×3648 px) and has a working area of 20×15 mm² to 5000×4000 mm², which allows the sample to be observed with images taken at up to 17 Hz. The use of this system made it possible to examine the behaviour of the specimen with a hole during the tensile test when the specimen would crack and fail.

Figure 2 shows the complete experimental test stand. Figure 2a shows the testing machine with a load measuring device mounted on the

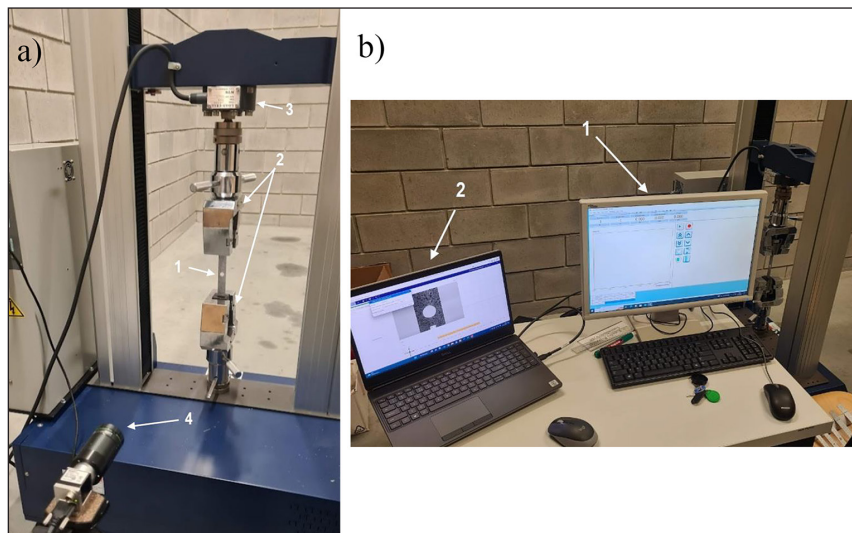


Fig. 2. Test stand: (a) testing machine with a fixed test specimen, (b) measuring software

upper crosshead and the wedge grips in which the test specimen was fixed. In front of the machine, a measuring camera of the Aramis non-contact optical system used was installed; it was oriented perpendicular to the face of the specimen that was painted in contrasting patterns. Before each test, the camera was calibrated to ensure that the images captured at 17 Hz were of the highest possible quality. Figure 2b shows the experimental test recording rig equipped with dedicated software for running testing machine (Fig 2b:1) and Aramis non-contact measuring system (Fig. 2b:2). Tests were performed using the standard ASTM D5766 open hole polymer matrix composite laminate tensile strength test method [58].

THE NUMERICAL ANALYSIS

The FEM analysis was performed using the commercial version of the Abaqus system [59]. An adequate FEM model reproducing the experimental sample was prepared [60–63]. The FEM model of the composite was made by modelling each layer individually to obtain a solid with the dimensions of 20×120×0.131 mm (width × length × thickness). Each layer was assigned material properties of the engineering constants type, according to Table 1. The layers were then stacked on top of each other, yielding a stack of 8 layers. The layers were assigned material orientation according to the laminate configuration [0/90/0/90/90/0/90/0]. The individual layers were

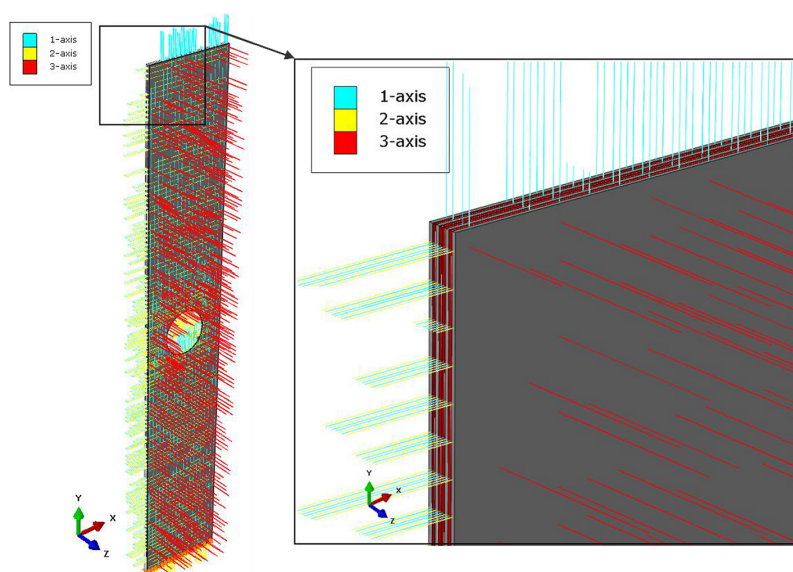


Fig. 3. FEM model of the laminate

tied together, and the cohesion between them was determined. The FEM model had the dimensions of 20 mm (width) × 120 mm (height) × 1.048 mm (thickness) and was a layered structure. Figure 3 presents the FEM model of the CFRP material together with the fibre arrangement in each layer.

To accelerate the FEM process time, the numerical model was limited to the experimentally tested area of the specimen (20×120×1.048 mm plate). Boundary conditions were defined for the upper and lower cross-sectional surfaces of the FEM model. The lower surface was fully fixed by blocking $U_x=U_y=U_z=UR_x=UR_y=UR_z=0$ (all degrees of freedom). The upper surface was fixed by blocking $U_x=U_z=0$ (two translational degrees of freedom) and $UR_x=UR_y=UR_z=0$ (three rotational degrees of freedom). To apply the tensile load, a reference point RP was established at the midpoint of the upper surface and was linked by a kinematic coupling relation to the upper surface, thus giving all degrees of freedom. A load of 10 kN was defined at the reference point according to the Y-vector expression, as shown in Figure 4a. In the XFEM analysis, a contact interaction property was assigned to each layer of the laminate to define the behaviour of the compression fracture surfaces. The interactions between the layers in the FEM model are represented in Figure 4b. The numerical model was discretised using the C3D8R hex solid elements having linear interpolation with 8 nodes and reduced integration. For

the structural mesh, partitions of the FEM model were made, and a density of the FEM mesh was increased around the circumference of the circular hole. The discretised model had 20480 elements and 43840 nodes (Fig. 4c). The finite element size was adopted based on the preliminary numerical analysis, which proved that decreasing the finite element size did not affect the quality of the numerical results.

The use of the XFEM allows us to study the crack initiation and propagation without re-meshing the model [23]. For crack analysis, enrichment functions usually consist of asymptotic near-tip functions capturing the singularity around the crack tip and a discontinuous function representing the displacement jump on the crack surfaces. The nodal displacement vector enrichment function u [64,65]:

$$u = \sum_{I=1}^N N_I(X) \left[u_I + H(X)A_I + \sum_{\alpha=1}^4 F_{\alpha}(X)B_I^{\alpha} \right] \quad (1)$$

where: $N_I(X)$ – nodal shape function;
 u_I – nodal displacement vector of a continuous part of the FEM solution;
 $H(X)$ – discontinuous jump function across the crack surface;
 A_I – nodal vector of degrees of freedom;
 $F_{\alpha}(X)$ – elastic asymptotic function of the crack tip;

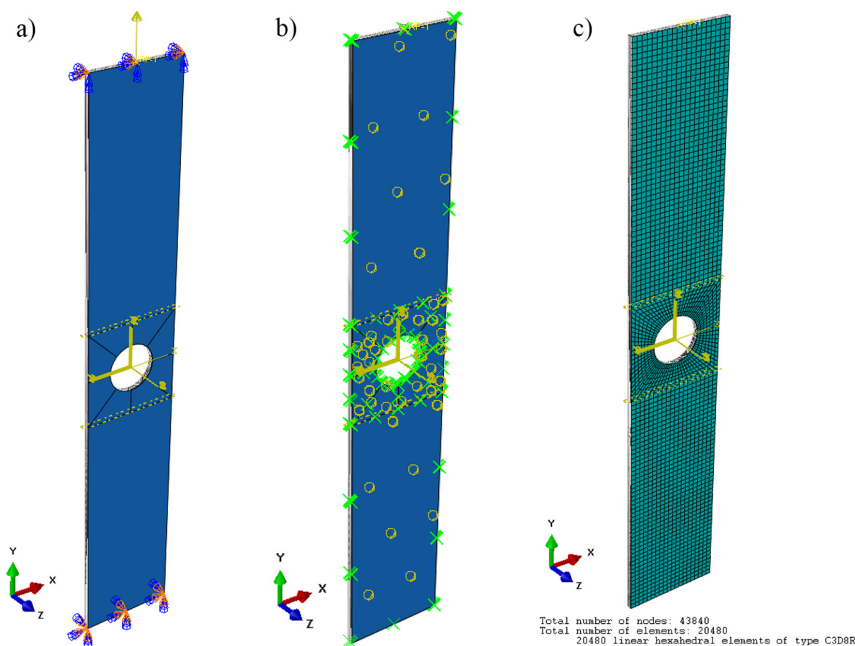


Fig. 4. Numerical model: (a) implementation of boundary conditions, (b) layer-by-layer interactions, (c) model discretisation

B_I^α – nodal vector of degrees of freedom. The first term of the formula is applied to all nodes in the model. The second term is applied to nodes whose shape function support is intersected by the crack interior. The third term is only used for nodes whose shape function support is intersected by the crack apex – Figure 5.

Discontinuous function of jump across the fracture surface $H(X)$ could be expressed as follows [65]:

$$H(X) = \begin{cases} 1 & \text{if } (X - X^*) \cdot n \geq 0 \\ -1 & \text{otherwise} \end{cases} \quad (2)$$

where: X – sample point (Gaussian);
 X^* – point on the crack closest to X ;
 n is the unit outward normal to the crack at X^* .

Asymptotic function of the crack tip for an elastic material is described by the following relation [23]:

$$F_\alpha(X) = \begin{bmatrix} \sqrt{r} \sin \frac{\theta}{2}, \sqrt{r} \cos \frac{\theta}{2}, \\ \sqrt{r} \sin \theta \sin \frac{\theta}{2}, \sqrt{r} \sin \theta \cos \frac{\theta}{2} \end{bmatrix} \quad (3)$$

where: r, θ – polar coordinates of the system whose origin is at the crack tip;
 $\theta = 0$ – finally tangent to the crack.

The asymptotic functions of the crack tip are only considered in the modelling stationary cracks using Abaqus/Standard. In contrast, moving cracks can be modelled using one of two alternative approaches: the cohesive segment approach or the linear elastic fracture mechanics (LEFM) approach [23]. Crack initiation is defined up to

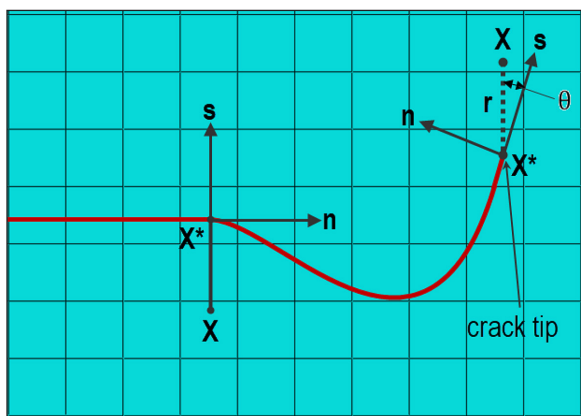


Fig. 5. The normal and the tangential vectors for the smooth fracture

the onset of cohesive degradation in the enriched component. In contrast, the degradation stage occurs when the stresses or strains meet specified crack initiation criteria. One such criterion is the maximum principal stress (MAXPS) criterion which is defined as follows [27]:

$$F = \frac{\langle \sigma_{MAX} \rangle}{\sigma_{MAX}^0} \quad (4)$$

where: σ_{MAX}^0 – the maximum permissible principal stress.

Maximum principal stress ratio $\langle \sigma_{MAX} \rangle$ shown in the Macaulay brackets assumes that the damage begins when a value of 1 is reached [27]:

$$\begin{cases} \langle \sigma_{MAX} \rangle = 0 & \text{if } \sigma_{MAX} < 0 \\ \langle \sigma_{MAX} \rangle = \sigma_{MAX} & \text{if } \sigma_{MAX} \geq 0 \end{cases} \quad (5)$$

RESULTS AND DISCUSSION

The study was conducted using two independent approaches: experiments and numerical analysis by FEM method. Numerical results obtained from the FEM analysis in the form of the maximum stress field in longitudinal direction of plate are presented in Figure 6. The numerical analysis showed that, at this stage, the highest tensile stresses in longitudinal direction of specimen were located symmetrically on both sides of the circular hole. The maximum tensile stresses were located in the laminate layers with the 0° fibre configuration relative to longitudinal direction of the specimen. The results presented in Figure 6 are given for the non-failure stresses in the composite $\sigma_{t,S11} = 1828.8$ MPa, i.e. they do not exceed the limit tensile stress in the longitudinal direction $\sigma_{t,S11} \leq F_{T1} = 1867.2$ MPa (Table 1).

The initiation of a damage in the composite structure was observed once the F_{T1} longitudinal

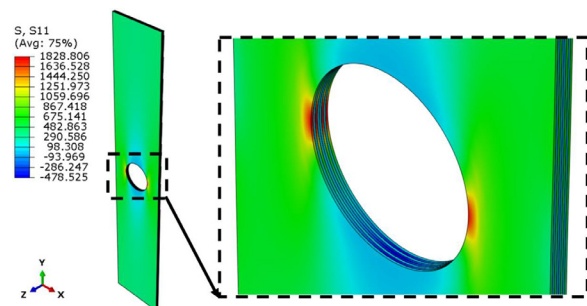


Fig. 6. Stress zone of a CFRM material before damage

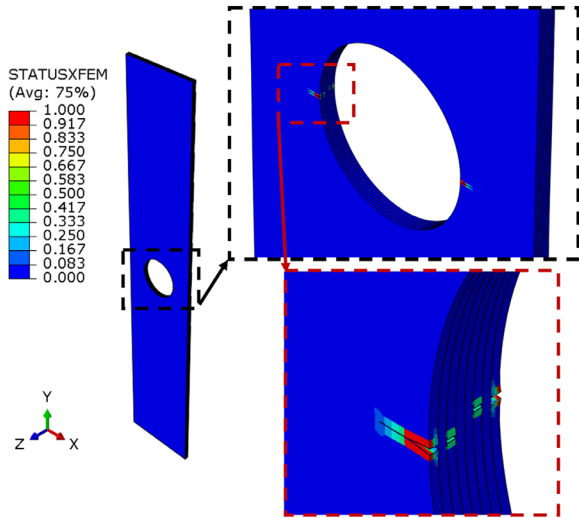


Fig. 7. Damage and crack propagation in a composite structure

strength limit was exceeded. This was followed by crack propagation in individual laminate layers. Figure 7 presents a bitmap showing the beginning of fracture process in studied laminated material structure. Cracking process was determined

numerically using the XFEM. The cracking initiated when a value of 1 was reached according to maximum principal stress ratio criterion. The damage process of the composite structure started with symmetric cracking of the outermost layers of the laminate with the 0° fibre configuration in the region of the circular hole, as presented in Figure 7. It should be added that the achievement of the damage criterion triggered the cracking of other laminate layers with the 0° fibre configuration (layers 3 and 6).

The Aramis non-contact optical measuring system was used in the experiments to measure specimen displacement. The measuring system made it possible to generate a graphic displacement map superimposed on the real plate. Figure 8 shows a comparison of all cases taken for analysis in terms of specimen elongation during tensile testing. The proposed experimental method allowed the elongation of the specimens to be measured before complete failure. The elongation of the experimental samples was in the range $<0.691\text{--}0.809\text{ mm}>$ and represented the

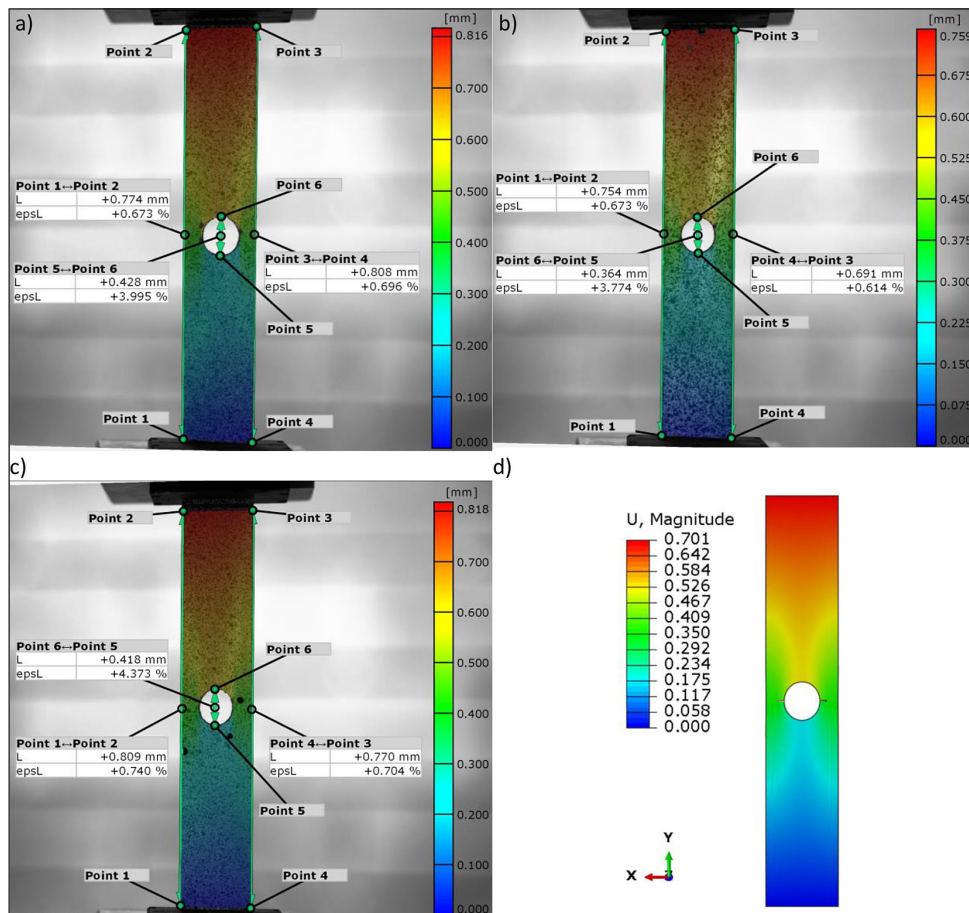


Fig. 8. Longitudinal elongation maps of a plate with a hole: (a) real sample 1, (b) real sample 2, (c) real sample 3, (d) FEM model

percentage elongation of the plate ranging $<0.61\text{--}0.69\%>$, as presented in Figures 8a-c. In addition, the elongation of the real plates in the hole region was measured, with its value ranging $<0.364\text{ mm (3.8\%)} - 0.428\text{ mm (4\%)}>$ (Figs. 8a-c). Experimental was compared with the numerical analysis. Deformations observed for both test methods were found to be consistent. The maximum elongation of the numerical sample before failure was 0.701 mm (Fig. 8d), which agreed with the experimental measurements. The results showed quantitative and qualitative agreement between the numerical analysis and the experiment. The results confirmed the agreement of the proposed FEM model with the experimental sample.

Experimental and numerical tests were conducted in the full range of tensile loads up to complete failure of the composite. Figures 9a-c shows the experimental modes of failure of plate with a circular open hole. As expected, for all cases, the real specimen cracked in the region where it had previously been weakened by the hole. The

fracture path passed across the plate, along its length. Parallel numerical analysis showed a consistent failure mode, as presented in Figure 9d. The crack propagation in the FEM model (Fig. 7) initiated in the same region as in the experiment (Figs. 9a-c) and progressed in the transverse direction. The strength of plate depended on strength of the layers with the 0° fibre configuration, as they were the most stressed in the tensile test. The damage of the composite structure progressed horizontally and consisted of cracking and subsequent delamination of individual layers.

The tensile load as a function of specimen elongation was calculated experimentally. This made it possible to determine the working paths of plates tensile in the full load range until failure (Figs. 10a-c). Adequate characteristics were determined for the numerical model, as presented in Figure 10d. This approach made it possible to represent graphically the damage load corresponding to initiation of laminate fracture and failure load causing the complete failure of the composite

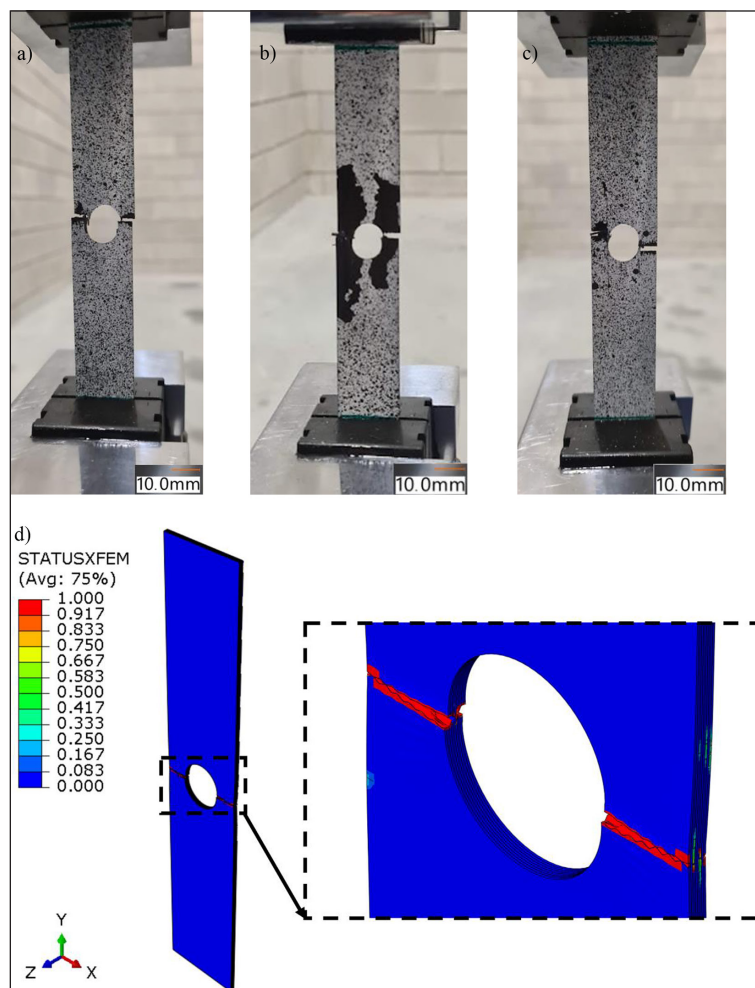


Fig. 9. Complete failure of a laminated structure: (a) real plate 1, (b) real plate 2, (c) real plate 3, (d) FEM model

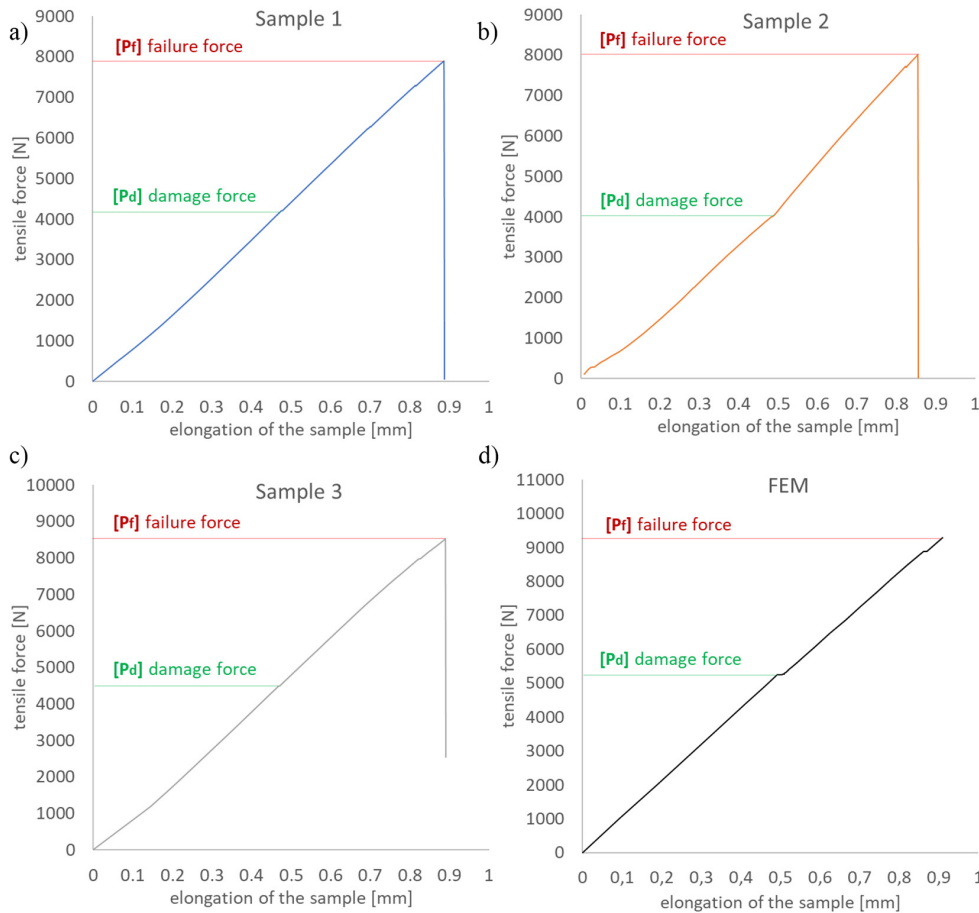


Fig. 10. Working paths of a laminated structure: (a) real plate 1, (b) real plate 2, (c) real plate 3, (d) FEM model

structure. The damage load P_d corresponded to the first sudden increase in elongation observed along the working path, while the experimental failure load P_f was determined at the point of a sudden decrease in the tensile load (Figs. 10a-c). In the numerical analysis, P_d was determined in the same way as in the experiment, while P_f was determined at the point of the highest tensile load.

Table 2 presents all experimental and numerical damage load and failure load values. The experimental values of the laminate damage initiation load $P_{d(EXP)}$ ranged $\langle 4099.2\text{--}4443.9\text{ N}\rangle$, while the numerical $P_{d(FEM)} = 5153.3\text{ N}$. The failure loads corresponding to the complete failure of the composite due to fracture were $P_{f(EXP)} = \langle 7735.1\text{--}8264.5\text{ N}\rangle$ and $P_{f(FEM)} = 9298.7\text{ N}$. Based on the results, the percentage increase in the failure load of the composite structure P_f relative to the failure

initiation load P_d was determined. After reaching the damage load, the real structure could still carry the load increased by $\langle 85\text{--}90\% \rangle$.

Figure 11 shows the comparison of the numerical and experimental working paths. The numerical results show agreement with the experimental findings. The numerical working path of the plate is characterised by a higher stiffness. Compared to the experiment, the maximum increase in the stiffness of the FEM model is 11%. The difference in stiffness between the numerical and experimental paths may result from geometrical imperfections, the occurrence of which is unavoidable in real structures.

Table 3 shows the percentage differences between the experimental and numerical damage and failure loads. The maximum difference was observed for the damage loads of $P_{d(FEM)}$ and

Table 2. Damage load and failure load of a composite structure

Load	FEM	Sample 1	Sample 2	Sample 3
P_d [N]	5153.3	4185.9	4099.2	4443.9
P_f [N]	9298.7	7735.1	7801.5	8264.5
	80%	85%	90%	86%

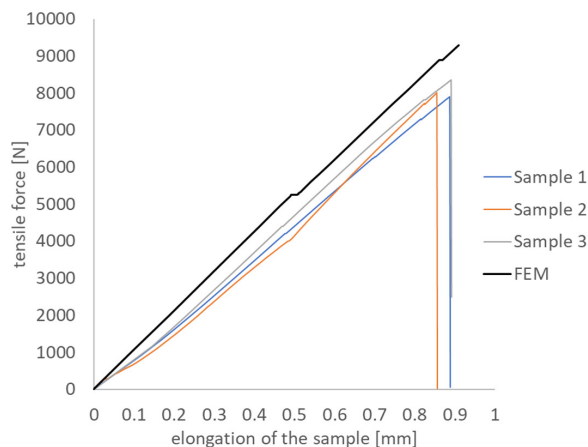


Fig. 11. Numerical and experimental and working paths of a plate

Table 3. Percentage differences in damage and failure loads

Load	FEM/Sample 1	FEM/Sample 2	FEM/Sample 3
P_d	19%	20%	14%
P_f	17%	16%	11%

$P_{d(EXP)Sample2}$ and amounted to 20%. In contrast, the smallest difference of 11% was observed between $P_{f(FEM)}$ and $P_{f(EXP)Sample3}$. Quantitatively, the differences between the experiment and the FEM were within acceptable engineering error and did not exceed 20%, which shows agreement between the numerical model and the experiment.

CONCLUSIONS

The study analysed the behaviour of a tensile composite plate with the hole open in several aspects. The first consisted of examining the plate with the hole before the failure symptoms. Then the damage initiation, the initial crack and the delamination of the laminate layers were analysed. Then, at the last stage, the crack propagation leading to the fracture of all laminate layers (complete destruction of the composite structure).

The maximum tensile stresses were located in the laminate layers with the 0° fibre configuration relative to the longitudinal direction of the specimen. The damage process of the composite structure initiated as symmetrical cracking of the outer layers of the laminate with the 0° fibre configuration in the circular hole region.

The maximum elongation of the numerical specimen before failure was 0.701 mm and agreed with the experimental measurements.

The deformations observed for both test methods were found to be consistent.

For all cases, the real sample cracked in the circular hole region. The damage of the composite structure progressed horizontally and consisted of cracking and subsequent delamination of individual layers.

The experimental values of the laminate failure initiation load $P_{d(EXP)}$ ranged <4099–4444 N>, while the numerical $P_{d(FEM)} = 5153$ N. The failure load corresponding to complete failure of the composite due to fracture was $P_{f(EXP)} = <7735–8264$ N> and $P_{f(FEM)} = 9299$ N. After reaching the damage load, the tensile tested real structure could still carry the load increased by <85–90%>.

The experimental working paths showed agreement with the numerical results. The numerical working path of the plate was characterised by a higher stiffness. Compared to the experiment, the maximum increase in the stiffness of the FEM model was 11%. This was based on the numerical model being an idealised, defect-free structure.

For validation, percentage differences between the numerical results and the experimental values of damage load and failure load were determined. The differences for the damage load ranged <14–20%>, while for the failure load they were <11–17%>. The differences did not exceed the acceptable engineering error of 20%.

The experimental and numerical results showed qualitative and quantitative agreement. The results also confirmed that the developed FEM/XFEM numerical model reproduced the experimental conditions accurately. The developed research methodology contributes to a more precise modelling and analysis of real composite structures. The results obtained also provide detailed information of practical relevance, allowing effective optimisation of the composite structure to be carried out according to the structural requirements.

Future research will investigate the influence of composite material parameters, e.g. layer configuration, number of layers and hole size, on crack propagation. As part of the research, experiments will be performed first and then they will be validated numerically using the currently popular finite element method (FEM) [66–74]. The research methodology and conclusions described in this paper will be used in the future study.

REFERENCES

- Campbell, F.C. *Manufacturing Technology for Aerospace Structural Materials*; 1st ed.; Elsevier: Amsterdam ; Boston, 2006.
- Kassapoglou, C. *Design and Analysis of Composite Structures: With Applications to Aerospace Structures*; AIAA education series; 1st ed.; American Institute of Aeronautics and Astronautics: Reston, Va. : United Kingdom : b John Wiley & Sons, 2010.
- Parlapalli, M.R., Soh, K.C., Shu, D.W., Ma, G. Experimental Investigation of Delamination Buckling of Stitched Composite Laminates. *Composites Part A: Applied Science and Manufacturing*. 2007; 38: 2024–2033. DOI: 10.1016/j.compositesa.2007.05.001
- Turvey, G.J., Zhang, Y. A Computational and Experimental Analysis of the Buckling, Postbuckling and Initial Failure of Pultruded GRP Columns. *Computers & Structures*. 2006; 84: 1527–1537. DOI: 10.1016/j.compstruc.2006.01.028
- Teter, A., Kolakowski, Z. Coupled Dynamic Buckling of Thin-Walled Composite Columns with Open Cross-Sections. *Composite Structures*. 2013; 95: 28–34. DOI: 10.1016/j.compstruct.2012.08.006
- Kubiak, T., Mania, R.J. Hybrid versus FR Laminate Channel Section Columns – Buckling and Postbuckling Behaviour. *Composite Structures*. 2016; 154: 142–149. DOI: 10.1016/j.compstruct.2016.07.040.
- Gliszczynski, A., Kubiak, T., Wawer, K. Barely Visible Impact Damages of GFRP Laminate Profiles – An Experimental Study. *Composites Part B: Engineering*. 2019; 158: 10–17. DOI: 10.1016/j.compositesb.2018.09.044
- Gliszczynski, A., Wiącek, N. Experimental and Numerical Benchmark Study of Mode II Interlaminar Fracture Toughness of Unidirectional GFRP Laminates under Shear Loading Using the End-Notched Flexure (ENF) Test. *Composite Structures*. 2021; 258: 113190. DOI: 10.1016/j.compstruct.2020.113190
- Debski, H., Kubiak, T., Teter, A. Experimental Investigation of Channel-Section Composite Profiles' Behavior with Various Sequences of Plies Subjected to Static Compression. *Thin-Walled Structures*. 2013; 71: 147–154. DOI: 10.1016/j.tws.2013.07.008
- Wong, P.M.H., Wang, Y.C. An Experimental Study of Pultruded Glass Fibre Reinforced Plastics Channel Columns at Elevated Temperatures. *Composite Structures*. 2007; 81: 84–95. DOI: 10.1016/j.compstruct.2006.08.001
- Orifici, A.C., Thomson, R.S., Degenhardt, R., Kling, A., Rohwer, K., Bayandor, J. Degradation Investigation in a Postbuckling Composite Stiffened Fuselage Panel. *Composite Structures*. 2008; 82: 217–224. DOI: 10.1016/j.compstruct.2007.01.012
- Kim, S.-C., Kim, J.S., Yoon, H.-J. Experimental and Numerical Investigations of Mode I Delamination Behaviors of Woven Fabric Composites with Carbon, Kevlar and Their Hybrid Fibers. *Int. J. Precis. Eng. Manuf.* 2011; 12: 321–329. DOI: 10.1007/s12541-011-0042-7
- Carlsson, L.A., Adams, D.F., Pipes, R.B. *Experimental Characterization of Advanced Composite Materials*; 4. ed.; CRC Press: Boca Raton, Fla., 2014.
- Fascetti, A., Feo, L., Nisticò, N., Penna, R. Web-Flange Behavior of Pultruded GFRP I-Beams: A Lattice Model for the Interpretation of Experimental Results. *Composites Part B: Engineering*. 2016; 100: 257–269. DOI: 10.1016/j.compositesb.2016.06.058.
- Wysmulski, P. Load Eccentricity of Compressed Composite Z-Columns in Non-Linear State. *Materials*. 2022; 15: 7631. DOI: 10.3390/ma15217631
- Timoshenko, S., Gere, J.M. *Theory of Elastic Stability*; 2nd ed., Dover ed.; Dover Publications: Mineola, N.Y, 2009.
- Cheng, B., Zhao, J. Strengthening of Perforated Plates under Uniaxial Compression: Buckling Analysis. *Thin-Walled Structures*. 2010; 48: 905–914. DOI: 10.1016/j.tws.2010.06.001
- Jayashankarbabu B.S. Karisiddappa Stability Of Square Plate With Concentric Cutout. 2014. DOI: 10.5281/ZENODO.1337071.
- Lorenzini, G., Helbig, D., Silva, C., Real, M., Santos, E., Rocha, L. Numerical Evaluation of the Effect of Type and Shape of Perforations on the Buckling of Thin Steel Plates by Means of the Constructal Design Method. *IJHT*. 2016; 34: S9–S20. DOI: 10.18280/ijht.34Sp0102
- Durão, L.M.P., Matos, J.E., Loureiro, N.C., Esteves, J.L., Fernandes, S.C.F. Damage Propagation by Cyclic Loading in Drilled Carbon/Epoxy Plates. *Materials*. 2023; 16: 2688. DOI: 10.3390/ma16072688
- Joy Mathavan, J., Hassan, M.H., Xu, J., Franz, G. Hole Quality Observation in Single-Shot Drilling of CFRP/Al7075-T6 Composite Metal Stacks Using Customized Twist Drill Design. *J. Compos. Sci.* 2022; 6: 378. DOI: 10.3390/jcs6120378
- Wang, H., Wu, Y., Zhang, Y., Zhang, X. Influence of the Temperature-Dependent Characteristics of CFRP Mechanical Properties on the Critical Axial Force of Drilling Delamination. *Polymers*. 2023; 15: 680. DOI: 10.3390/polym15030680
- Elguedj, T., Gravouil, A., Combescure, A. Appropriate Extended Functions for X-FEM Simulation of Plastic Fracture Mechanics. *Computer Methods in Applied Mechanics and Engineering*. 2006; 195: 501–515. DOI: 10.1016/j.cma.2005.02.007
- Belytschko, T., Black, T. Elastic Crack Growth in Finite Elements with Minimal Remeshing. *Int. J. Numer. Meth. Engng.* 1999; 45: 601–620. DOI: 10.1002/(SICI)1097-0207(19990620)45:5<601::AID-NME598>3.0.CO;2-S

25. Melenk, J.M., Babuška, I. The Partition of Unity Finite Element Method: Basic Theory and Applications. *Computer Methods in Applied Mechanics and Engineering*. 1996; 139: 289–314. DOI: 10.1016/S0045-7825(96)01087-0
26. Nagashima, T., Suemasu, H. X-FEM Analyses of a Thin-Walled Composite Shell Structure with a Delamination. *Computers & Structures*. 2010; 88: 549–557. DOI: 10.1016/j.compstruc.2010.01.008
27. Abaqus HTML Documentation; 2016.
28. Liu, P.F., Gu, Z.P., Peng, X.Q., Zheng, J.Y. Finite Element Analysis of the Influence of Cohesive Law Parameters on the Multiple Delamination Behaviors of Composites under Compression. *Composite Structures*. 2015; 131: 975–986. DOI: 10.1016/j.compstruct.2015.06.058
29. Rabinovitch, O. Cohesive Interface Modeling of Debonding Failure in FRP Strengthened Beams. *J. Eng. Mech.* 2008; 134: 578–588. DOI: 10.1061/(ASCE)0733-9399(2008)134:7(578)
30. Fabbrocino, F., Funari, M.F., Greco, F., Lonetti, P., Luciano, R., Penna, R. Dynamic Crack Growth Based on Moving Mesh Method. *Composites Part B: Engineering*. 2019; 174: 107053. DOI: 10.1016/j.compositesb.2019.107053
31. Duarte, A.P.C., Díaz Sáez, A., Silvestre, N. Comparative Study between XFEM and Hashin Damage Criterion Applied to Failure of Composites. *Thin-Walled Structures*. 2017; 115: 277–288. DOI: 10.1016/j.tws.2017.02.020
32. Rozylo, P., Wymulski, P. Failure Analysis of Thin-Walled Composite Profiles Subjected to Axial Compression Using Progressive Failure Analysis (PFA) and Cohesive Zone Model (CZM). *Composite Structures*. 2021; 262: 113597. DOI: 10.1016/j.compstruct.2021.113597
33. Falkowicz, K., Ferdynus, M., Rozylo, P. Experimental and Numerical Analysis of Stability and Failure of Compressed Composite Plates. *Composite Structures*. 2021; 263: 113657. DOI: 10.1016/j.compstruct.2021.113657
34. Kubiak, T., Samborski, S., Teter, A. Experimental Investigation of Failure Process in Compressed Channel-Section GFRP Laminate Columns Assisted with the Acoustic Emission Method. *Composite Structures*. 2015; 133: 921–929. DOI: 10.1016/j.compstruct.2015.08.023
35. Banat, D., Mania, R.J. Failure Assessment of Thin-Walled FML Profiles during Buckling and Postbuckling Response. *Composites Part B: Engineering*. 2017; 112: 278–289. DOI: 10.1016/j.compositesb.2017.01.001
36. Barbero, E.J., Cosso, F.A. Determination of Material Parameters for Discrete Damage Mechanics Analysis of Carbon-Epoxy Laminates. *Composites Part B: Engineering*. 2014; 56: 638–646. DOI: 10.1016/j.compositesb.2013.08.084
37. Rozylo, P., Falkowicz, K. Stability and Failure Analysis of Compressed Thin-Walled Composite Structures with Central Cut-out, Using Three Advanced Independent Damage Models. *Composite Structures*. 2021; 273: 114298. DOI: 10.1016/j.compstruct.2021.114298
38. Rozylo, P. Comparison of Failure for Thin-Walled Composite Columns. *Materials*. 2021; 15: 167. DOI: 10.3390/ma15010167
39. Rozylo, P. Failure Phenomenon of Compressed Thin-Walled Composite Columns with Top-Hat Cross-Section for Three Laminate Lay-Ups. *Composite Structures*. 2023; 304: 116381. DOI: 10.1016/j.compstruct.2022.116381
40. Falkowicz, K. Experimental and Numerical Failure Analysis of Thin-Walled Composite Plates Using Progressive Failure Analysis. *Composite Structures*. 2023; 305: 116474. DOI: 10.1016/j.compstruct.2022.116474
41. Kurşun, A., Şenel, M., Enginsoy, H.M. Experimental and Numerical Analysis of Low Velocity Impact on a Preloaded Composite Plate. *Advances in Engineering Software*. 2015; 90: 41–52. DOI: 10.1016/j.advengsoft.2015.06.010
42. Wymulski, P., Debski, H. The Analysis of Sensitivity to Eccentric Load of Compressed Thin-Walled Laminate Columns.; Depok, Indonesia. 2019; 020006.
43. Wymulski, P. The Effect of Load Eccentricity on the Compressed CFRP Z-Shaped Columns in the Weak Post-Critical State. *Composite Structures*. 2022; 301: 116184. DOI: 10.1016/j.compstruct.2022.116184
44. Wu, M.Q., Zhang, W., Niu, Y. Experimental and Numerical Studies on Nonlinear Vibrations and Dynamic Snap-through Phenomena of Bistable Asymmetric Composite Laminated Shallow Shell under Center Foundation Excitation. *European Journal of Mechanics - A/Solids*. 2021; 89: 104303. DOI: 10.1016/j.euromechsol.2021.104303
45. Samborski, S., Gliszczyński, A., Rzekowski, J., Wiacek, N. Mode I Interlaminar Fracture of Glass/Epoxy Unidirectional Laminates. Part I: Experimental Studies. *Materials*. 2019; 12: 1607. DOI: 10.3390/ma12101607
46. Rogala, M., Gajewski, J. Numerical Analysis of Porous Materials Subjected to Oblique Crushing Force. *J. Phys.: Conf. Ser.* 2021; 1736: 012025. DOI: 10.1088/1742-6596/1736/1/012025
47. Grzejda, R., Warzecha, M., Urbanowicz, K. Determination of the Preload of Bolts for Structural Health Monitoring of a Multi-Bolted Joint: FEM Approach. *Lubricants*. 2022; 10: 75. DOI: 10.3390/lubricants10050075
48. Gliszczyński, A., Samborski, S., Wiacek, N., Rzekowski, J. Mode I Interlaminar Fracture of Glass/Epoxy Unidirectional Laminates. Part II: Numerical Analysis. *Materials*. 2019; 12: 1604. DOI: 10.3390/ma12101604
49. Jonak, J., Karpiński, R., Wójcik, A., Siegmund, M., Kalita, M. Determining the Effect of Rock Strength

- Parameters on the Breakout Area Utilizing the New Design of the Undercut/Breakout Anchor. *Materials*. 2022; 15: 851. DOI: 10.3390/ma15030851
50. Shao, S., Wu, Y., Fu, H., Feng, S., Zhang, J. Numerical Investigation on the Mechanical Properties of Vault Void Lining and Steel Plate Strengthening. *Materials*. 2023; 16: 789. DOI: 10.3390/ma16020789
 51. Hao, R., Wen, Z., Xin, H., Lin, W. Fatigue Life Prediction of Notched Details Using SWT Model and LEFM-Based Approach. *Materials*. 2023; 16: 1942. DOI: 10.3390/ma16051942
 52. Buccino, F., Cervellera, F., Ghidini, M., Marini, R., Bagherifard, S., Vergani, L.M. Isolating the Role of Bone Lacunar Morphology on Static and Fatigue Fracture Progression through Numerical Simulations. *Materials*. 2023; 16: 1931. DOI: 10.3390/ma16051931
 53. Wang, F., Wei, Z., Li, P., Yu, L., Huang, W. Initial Crack Propagation and the Influence Factors of Aircraft Pipe Pressure. *Materials*. 2019; 12: 3098. DOI: 10.3390/ma12193098
 54. Wymulski, P., Falkowicz, K., Filipek, P. Buckling State Analysis of Compressed Composite Plates with Cut-Out. *Composite Structures*. 2021; 274: 114345. DOI: 10.1016/j.compstruct.2021.114345
 55. Wymulski, P. Non-Linear Analysis of the Post-buckling Behaviour of Eccentrically Compressed Composite Channel-Section Columns. *Composite Structures*. 2023; 305: 116446. DOI: 10.1016/j.compstruct.2022.116446
 56. Falkowicz, K., Valvo, P. Influence of Composite Lay-Up on the Stability of Channel-Section Profiles Weakened by Cut-Outs – A Numerical Investigation. *Adv. Sci. Technol. Res. J.* 2023; 17: 108–115. DOI: 10.12913/22998624/156635
 57. Różyło, P., Smagowski, W., Paśnik, J. Experimental Research in the Aspect of Determining the Mechanical and Strength Properties of the Composite Material Made of Carbon-Epoxy Composite. *Adv. Sci. Technol. Res. J.* 2023; 17: 232–246. DOI: 10.12913/22998624/161598
 58. D30 Committee Test Method for Open-Hole Tensile Strength of Polymer Matrix Composite Laminates; ASTM International.
 59. Jonak, J., Karpinski, R., Wojcik, A., Siegmund, M. The Effect of Undercut Anchor Diameter on the Rock Failure Cone Area in Pullout Tests. *ASTRJ* 2022; 16.
 60. Jonak, J., Karpiński, R., Wójcik, A. Influence of the Undercut Anchor Head Angle on the Propagation of the Failure Zone of the Rock Medium—Part II. *Materials*. 2021; 14: 3880. DOI: 10.3390/ma14143880
 61. Nozdrzykowski, K., Grządziel, Z., Grzejda, R., Warzecha, M., Stępień, M. An Analysis of Reaction Forces in Crankshaft Support Systems. *Lubricants*. 2022; 10: 151. DOI: 10.3390/lubricants10070151
 62. Rzeczkowski, J., Paśnik, J., Samborski, S. Mode III Numerical Analysis of Composite Laminates with Elastic Couplings in Split Cantilever Beam Configuration. *Composite Structures*. 2021; 265: 113751. DOI: 10.1016/j.compstruct.2021.113751
 63. Grzejda, R. Thermal Strength Analysis of a Steel Bolted Connection under Bolt Loss Conditions. *EiN*. 2022; 24: 269–274. DOI: 10.17531/ein.2022.2.8
 64. Remmers, J., Deborst, R., Needleman, A. The Simulation of Dynamic Crack Propagation Using the Cohesive Segments Method. *Journal of the Mechanics and Physics of Solids*. 2008; 56: 70–92. DOI: 10.1016/j.jmps.2007.08.003
 65. Ventura, G., Benvenuti, E. Equivalent Polynomials for Quadrature in Heaviside Function Enriched Elements: Equivalent Polynomials For Heaviside Function Enriched Elements. *Int. J. Numer. Meth. Engng.* 2015; 102: 688–710. DOI: 10.1002/nme.4679
 66. Rogala, M., Gajewski, J., Ferdynus, M. The Effect of Geometrical Non-Linearity on the Crashworthiness of Thin-Walled Conical Energy-Absorbers. *Materials*. 2020; 13: 4857. DOI: 10.3390/ma13214857
 67. Jonak, J., Karpiński, R., Wójcik, A. Influence of the Undercut Anchor Head Angle on the Propagation of the Failure Zone of the Rock Medium. *Materials*. 2021; 14: 2371. DOI: 10.3390/ma14092371
 68. Jonak, J., Karpiński, R., Wójcik, A. Numerical Analysis of Undercut Anchor Effect on Rock. *J. Phys.: Conf. Ser.* 2021; 2130: 012011. DOI: 10.1088/1742-6596/2130/1/012011
 69. Jonak, J., Karpiński, R., Wójcik, A. Numerical Analysis of the Effect of Embedment Depth on the Geometry of the Cone Failure. *J. Phys.: Conf. Ser.* 2021; 2130: 012012. DOI: 10.1088/1742-6596/2130/1/012012
 70. Jaszak, P., Skrzypacz, J., Borawski, A., Grzejda, R. Methodology of Leakage Prediction in Gasketed Flange Joints at Pipeline Deformations. *Materials*. 2022; 15: 4354. DOI: 10.3390/ma15124354
 71. Rogala, M., Gajewski, J., Gawdzińska, K. Crashworthiness Analysis of Thin-Walled Aluminum Columns Filled with Aluminum–Silicon Carbide Composite Foam. *Composite Structures*. 2022; 299: 116102. DOI: 10.1016/j.compstruct.2022.116102
 72. Samborski, S., Rzeczkowski, J. Numerical Modeling and Experimental Testing of the DCB Laminated Composite Beams with Mechanical Couplings.; Lublin, Poland. 2018; 080010.
 73. Rzeczkowski, J., Paśnik, J., Samborski, S. Corrigendum to “Mode III Numerical Analysis of Composite Laminates with Elastic Couplings in Split Cantilever Beam Configuration.” *Composite Structures*. 2021; 266: 113920. DOI: 10.1016/j.compstruct.2021.113920
 74. Paśnik, J., Samborski, S., Rzeczkowski, J. Application of the CZM Technique to Delamination Analysis of Coupled Laminate Beams. *IOP Conf. Ser.: Mater. Sci. Eng.* 2018; 416: 012075. DOI: 10.1088/1757-899X/416/1/012075